Transactions on Machine Intelligence 5(3) (2022) 210-221

ISSN Online: 2821-1693

Transactions on Machine Intelligence

Journal Homepage: https://tmachineintelligence.ir/index.php/TMI

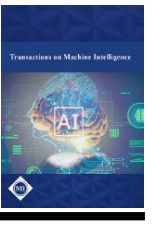

Effect of Grading Index on The Stress Response of a Rotating FGM Hollow Cylinder with Functionally Graded Piezoelectric Layers

M. Saadatfar[1,*], Y. Bik Iravani[2], W.T. Saleh[2], I. K. I. Al-hamadani[2], K.H. Ayish[2]

[1] Associate Prof. of Mechanical Engineering, Department of Mechanical Engineering, University of Qom, Qom, Iran
[2] MSc. Student of Mechanical Engineering Department of Mechanical Engineering, University of Qom, Qom, Iran

ARTICLE INFO

Article History:
Received 10 June 2022
Received in revised form 29 August 2022
Accepted 29 September 2022
Available online 30 September 2022

Keywords:
Grading Index, Functionally Graded Piezoelectric, Long Hollow Cylinder, Stress Distribution

ABSTRACT

This study presents a comprehensive analytical investigation into the thermo-electro-elastic response of a rotating long hollow cylinder composed of a functionally graded material (FGM), with radially polarized functionally graded piezoelectric material (FGPM) layers perfectly bonded to its inner and outer surfaces. The cylinder is subjected to simultaneous thermal, electrical, and mechanical loadings, providing a realistic simulation of operational conditions in advanced electromechanical systems. The material properties of both the FGM cylinder and the FGPM layers are assumed to vary continuously along the radial direction according to a power-law distribution, while Poisson's ratio remains constant in the FGM region. The structure is analyzed under steady-state conditions while rotating at a constant angular velocity around its central axis. Closed-form analytical expressions are derived for the radial displacement, stress components, and electric potential using the theory of elasticity and electro-mechanics. The results are validated through parametric studies that explore the effects of key variables such as the material gradation index, angular velocity, thickness ratio, applied electrical voltage, and boundary temperatures. Numerical simulations illustrate how these parameters influence the stress distribution and overall structural behavior. The findings offer valuable design insights for advanced smart structures and rotating piezoelectric devices, emphasizing the importance of functional grading in enhancing mechanical integrity and electromechanical coupling performance under complex operational environments.

1. INTRODUCTION

The use of piezoelectric layers as distributed sensors and actuators has garnered significant attention in modern engineering due to their direct and inverse effects. Functionally graded piezoelectric material (FGPM) is a type of piezoelectric material whose composition and properties vary continuously in specific directions. FGPMs are intentionally designed composite materials tailored to exhibit desirable properties for specific applications.

Innovative structures incorporating functionally graded materials (FGMs) bonded with piezoelectric actuators and sensors demonstrate adaptive responses to environmental changes. Consequently, the integration of piezoelectric

* Corresponding Author: m.saadatfar@gmail.com
Associate Prof. of Mechanical Engineering, Department of Mechanical Engineering, University of Qom, Qom, Iran

http://dx.doi.org/10.47176/TMI.2022.210

materials with FGMs or other composites has become a central focus in the field of smart materials and structures, leading to the publication of numerous studies. For instance, Alibeigloo [1, 2] investigated the static analysis of functionally graded cylindrical shells with piezoelectric layers under various boundary conditions. Using classical shell theory, Liew et al. [3] and He et al. [4] explored the active control of FGM shells using piezoelectric sensors and actuators. Wang [5] examined the dynamic electromechanical behavior of a triple-layer infinite piezoelectric composite cylinder with imperfect interfaces. Shen and Noda [6] analyzed the post-buckling behavior of an FGM cylindrical shell with piezoelectric actuators, while another study [7] presented thermo-electro-elastic analytical solutions for a long functionally graded hollow cylinder bonded to FGPM layers.

Rotating cylinders and disks also play critical roles in rotating machinery and structural applications. For instance, El-Naggar et al. [8] studied thermal stresses in a rotating non-homogeneous orthotropic hollow cylinder. Eraslan and Akis [9] derived plane strain and plane stress solutions for functionally graded rotating solid shafts and disks. Saadatfar et al. [10, 11] analyzed stress distributions and displacements in various functionally graded rotating structures, including porous magneto-electro-elastic hollow cylinders under axisymmetric thermo-magneto-electro-mechanical loading.

Despite these advancements, the thermo-electro-elastic analysis of a rotating functionally graded hollow cylinder bonded with FGPM layers has yet to be addressed. This paper presents an analytical solution for such a system, specifically a rotating FGM hollow cylinder of infinite length, surface-bonded with radially polarized FGPM layers. The model considers pressure, electrical excitation, and thermal conditions. Material properties of the FGM cylinder and FGPM layers are assumed to follow a radial power-law distribution, with a constant Poisson's ratio for the FGM hollow cylinder. The hybrid cylinder rotates about its axis at a constant angular velocity. Analytical solutions are derived to evaluate the stress, displacement, and electric potential distributions. Numerical results illustrate the effects of material inhomogeneity, thermo-electro-mechanical boundary conditions, angular velocity, and thickness ratios on the static behavior of the FGM shell.

2. BASIC FORMULATIONS OF THE PROBLEM

An infinitely long functionally graded hollow cylinder, as illustrated in Fig. 1, is considered, featuring nonhomogeneous mechanical properties that vary radially. The system is analyzed using a cylindrical coordinate system (r,θ,z)(r, \theta, z). The FGM cylinder is perfectly bonded to functionally graded piezoelectric layers, serving as a sensor on the outer surface and an actuator on the inner surface. The cylinder rotates around its axis with a constant angular velocity ω\omega, and it is subjected to axisymmetric thermal, mechanical, and electrical loadings.

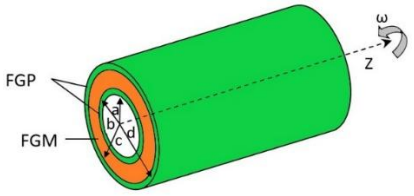

Fig. 1 Rotating multi layered hollow cylinder

2.1. Heat conduction problem

In this section, the symmetric, steady-state heat transfer equation may be solved for the assumed boundary conditions in the cylindrical coordinate system for FGM cylinder bonded with two FGPM layers. The heat conduction equation in the steady-state condition for the one-dimension problem without internal heat source in the cylindrical coordinate is expressed as:

$$\frac{1}{r}\frac{\partial}{\partial r}\left(rk(r)\frac{\partial T(r)}{\partial r}\right) = 0, (a \le r \le d), \tag{1}$$

where k(r) is the thermal conduction coefficient of the hollow cylinder in the radial direction. Thermal conduction coefficients of FGM cylinder, inner FGPM layer and outer FGPM layer can be expressed as $k(r) =$

$k_{fgm}r^{\eta}$, $k(r) = k_i r^{\beta}$ and $k(r) = k_o r^{\beta}$ where k_{fgm}, k_i and k_o are thermal conduction coefficients in the inner surface of FGM, inner FGPM and outer FGPM layers,, respectively. Also, η and β are in-homogeneity parameters of FGM and FGPM layers, respectively. Now Eq. (1) becomes:

$$\frac{1}{r}\frac{\partial}{\partial r}\left[r^{\theta+1}\frac{\partial T\ (r)}{\partial r}\right] = 0\theta = \beta, \eta. \tag{2}$$

By integrating twice, the solution of Eq. (2) for every layer can be expressed as:

$$\begin{aligned} T_i(r) &= w_1^i r^{-\beta} + w_2^i, \\ T_{fgm}(r) &= w_3 r^{-\eta} + w_4, \\ T_o(r) &= w_1^o r^{-\beta} + w_2^o \end{aligned} \tag{3}$$

where Ti, To and Tfgm are temperature distributions in the inner FGPM, outer FGPM and FGM layer, respectively. wi (i=1, 2, 3, 4) are unknown coefficients can be found using boundary conditions. The boundary conditions and continuity conditions can be expressed as [12]:

$$\begin{aligned} &T_i(r)|_{r=a} = T_0, T_i(r)|_{r=b} = T_{fgm}(r)\big|_{r=b}, T_o(r)|_{r=c} = T_{fgm}(r)\big|_{r=c}, \\ &q_i(r)|_{r=b} = q_{fgm}(r)\big|_{r=b}, q_o(r)|_{r=c} = q_{fgm}(r)\big|_{r=c}, [\partial T_o(r)/\partial r + hT_o(r)]|_{r=d} = 0 \end{aligned} \tag{4}$$

where h is the ratio of the convective heat-transfer coefficient of the cylinder and the surrounding medium and qj (j=i, o, fgm) are heat flux.

2.2. FGM layer

In the symmetric state, the nonzero components of displacement and thermal distribution can be denoted as u = u(r) and T=T(r). The equation of motion of the long FGM hollow cylinder in plane strain state and absence of body forces, is expressed as:

$$\frac{\partial \sigma_r}{\partial r} + \frac{\sigma_r - \sigma_\theta}{r} + \rho_f r\omega^2 = 0 \tag{5}$$

where ρ_f is the mass density and ω is the angular velocity. By considering $\varepsilon_r = du/dr$ and $\varepsilon_\theta = u/r$, the stress–displacement relations for FGM cylinder are:

$$\begin{aligned} \sigma_r &= \frac{E(r)}{(1+\nu)(1-2\nu)}\left((1-\nu)\frac{du}{dr} + \nu\frac{u}{r}\right) - \frac{E(r)\alpha(r)T(r)}{(1-2\nu)}, \\ \sigma_\theta &= \frac{E(r)}{(1+\nu)(1-2\nu)}\left(\nu\frac{du}{dr} + (1-\nu)\frac{u}{r}\right) - \frac{E(r)\alpha(r)T\ (r)}{(1-2\nu)}. \end{aligned} \tag{6}$$

In the FGM layer, the Poisson's ratio ν is constant and the Young modulus, mass density and thermal expansion coefficient vary along the radial direction according to a power law ($E(r) = E_0 r^{\eta}, \rho_f(r) = \rho_f^0 r^{\eta}, \alpha(r) = \alpha_0 r^{\eta}$) [13]. where E_0, ρ_f^0 and α_0 are material constants and η is the inhomogeneous constant. Substituting last Eq. and Eq. (6) into Eq. (5) gives:

$$\frac{d^2u}{dr^2}+(\eta+1)\frac{1}{r}\frac{du}{dr}+\left(\frac{\eta\nu}{1-\nu}-1\right)\frac{1}{r^2}u = -\frac{(1+\nu)(1-2\nu)\rho_f^0\omega^2}{E_0(1-\nu)}r+\frac{(1+\nu)\alpha_0}{1-\nu}\left(2\eta r^{\eta-1}T(r)+r^{\eta}\frac{dT(r)}{dr}\right). \tag{7}$$

Substituting from Eq. (3) into Eq. (7), yields:

$$\frac{d^2u}{dr^2}+(\eta+1)\frac{1}{r}\frac{du}{dr}+\left(\frac{\eta\nu}{1-\nu}-1\right)\frac{1}{r^2}u = -\frac{(1+\nu)(1-2\nu)\rho_f^0\omega^2}{E_0(1-\nu)}r \quad +\frac{(1+\nu)\eta\alpha_0 w_3}{1-\nu}r^{-1}+\frac{2(1+\nu)\eta\alpha_0 w_4}{1-\nu}r^{\eta-1}. \tag{8}$$

Assume that the complete solution of the basic displacement Eq. (8) may be expressed in the following form:

$$u = u_g + u_p. \tag{9}$$

It is obvious that the homogeneous solution to Eq. (8) can be obtained by assuming$u_g = Qr^{\eta_i}$. where Q is an arbitrary constant. Eq. (8) can be expressed as:

$$\eta_i^2+\eta\eta_i+(\frac{\eta\nu}{1-\nu}-1)=0. \tag{10}$$

For the numerical values (|η|≤ 2), only real, distinct roots will be obtained. However, these values for η do not necessarily represent a certain material, various η values are used to demonstrate the effect of in-homogeneity on the results. Thus, the characteristic Eq. (10) has two real roots η1 and η2 as follows:

$$\eta_1=-\frac{\eta}{2}-\sqrt{\frac{\eta^2}{4}-\frac{\nu\eta}{1-\nu}+1},\eta_2=-\frac{\eta}{2}+\sqrt{\frac{\eta^2}{4}-\frac{\nu\eta}{1-\nu}+1}. \tag{11}$$

Utilizing the homogeneous and particular solutions, we have:

$$u\ \ (r)=D_1r^{\eta_1}+D_2r^{\eta_2}+D_3r+D_4r^{\eta+1}+D_5r^3 b\le r\le c. \tag{12}$$

Since u(r) is known, the Eqs. (6) can be written as:

$$\begin{aligned}&\boldsymbol{\sigma_r=E_0[((1-\nu)\eta_1+\nu)D_1r^{\eta+\eta_1-1}+((1-\nu)\eta_2+\nu)D_2r^{\eta+\eta_2-1}+(D_3-(1+\nu)\alpha_0w_3)r^{\eta}}\\&\boldsymbol{+((\eta-\nu\eta+1)D_4-(1+\nu)\alpha_0w_4)r^{2\eta}+D_5(3-2\nu)r^{2+\eta}]/(1+\nu)(1-2\nu),}\\&\boldsymbol{\sigma_\theta=E_0[(\nu\eta_1+(1-\nu))D_1r^{\eta+\eta_1-1}+(\nu\eta_2+(1-\nu))D_2r^{\eta+\eta_2-1}+(D_3-(1+\nu)\alpha_0w_3)r^{\eta}}\\&\boldsymbol{+((\nu\eta+1)D_4-(1+\nu)\alpha_0w_4)r^{2\eta}+D_5(2\nu+1)r^{2+\eta}]/(1+\nu)(1-2\nu).}\end{aligned} \tag{13}$$

2.3. FGPM layer

The inner and outer layers are radially polarized functionally graded piezoelectric material. For the cylindrically symmetric state, the nonzero components of displacement, temperature distribution and electric potential can be denoted as u = u (r), T=T(r) and Φ = Φ(r), respectively. The constitutive equations for FGPM layers in the reference coordinate system are [14]:

$$\begin{aligned}\sigma_r &= c_{12}\frac{u}{r} + c_{11}\frac{\partial u}{\partial r} + e_{11}\frac{\partial \varphi}{\partial r} - \lambda_1 T(r),\\ \sigma_\theta &= c_{22}\frac{u}{r} + c_{12}\frac{\partial u}{\partial r} + e_{12}\frac{\partial \varphi}{\partial r} - \lambda_2 T(r),\\ D_r &= e_{12}\frac{u}{r} + e_{11}\frac{\partial u}{\partial r} - g_{11}\frac{\partial \varphi}{\partial r} + p_{11} T(r),\end{aligned} \tag{14}$$

where $\sigma_i(r)$ ($i = r, \theta$) and D_r are components of stress and electric displacement, respectively. c_{ij} , e_{1j}, g_{11} and p_{11} are the elastic, piezoelectric, dielectric, pyroelectric, constants, respectively. The equation of motion and the Maxwell equation in the absence of electric charge in the rotating piezoelectric layers are expressed as:

$$\frac{\partial \sigma_r}{\partial r} + \frac{\sigma_r - \sigma_\theta}{r} + \rho_p r\omega^2 = 0, \tag{15}$$

$$\partial[rD_r]/r\partial r = 0, \tag{16}$$

where ρ_p is the mass density of FGPM layer. All material constants are assumed to the same power-law dependence through the radius of the FGPM layer [12]. Solving Eqs. (16), yields:

$$D_r(r) = A_1/r, \tag{17}$$

where A_1 is unknown constant. Substituting Eqs. (17) into the Eqs. (14), gives:

$$\frac{\partial \varphi(r)}{\partial r} = \frac{e_{11}^0}{g_{11}^0}\frac{\partial u}{\partial r} + \frac{e_{12}^0}{g_{11}^0}\frac{u}{r} + \frac{p_{11}^0}{g_{11}^0}T(r) - \frac{A_1}{g_{11}^0}\frac{1}{r^{\beta+1}}. \tag{18}$$

$$\begin{aligned}\sigma_r &= C_1 r^\beta \frac{\partial u}{\partial r} + C_2 r^\beta \frac{u}{r} + C_3 r^\beta T(r) - C_4\frac{A_1}{r} - \lambda_1^0 r^{2\beta} T(r),\\ \sigma_\theta &= C_2 r^\beta \frac{\partial u}{\partial r} + C_5 r^\beta \frac{u}{r} + C_6 r^\beta T(r) - C_7\frac{A_1}{r} - \lambda_2^0 r^{2\beta} T(r),\end{aligned} \tag{19}$$

Substituting Eq. (19) into Eq. (15), the motion equation is expressed as:

$$\begin{aligned}&\frac{\partial^2 u}{\partial r^2} + (1+\beta)\frac{1}{r}\frac{\partial u}{\partial r} + W_1\frac{u}{r^2} = W_2 r^\beta \frac{T(r)}{r} + W_3\frac{T(r)}{r} + W_4 r^\beta \frac{\partial T(r)}{\partial r}\\ &+W_5\frac{\partial T(r)}{\partial r} + W_6 A_1 r^{-\beta-2} + W_7 r,\end{aligned} \tag{20}$$

Substituting the first equation of Eqs. (3) into Eq. (20), yields:

$$\frac{\partial^2 u}{\partial^2 r} + (1+\beta)\frac{1}{r}\frac{\partial u}{\partial r} + W_1\frac{u}{r^2} = W_9 r^{-1} + W_{10} r^{\beta-1} + W_{11} r^{-\beta-1} + W_6 A_1 r^{-\beta-2} + W_7 r, \tag{21}$$

Utilizing the homogeneous and particular solutions, we have:

$$\begin{aligned}u(r) = B_1 rm1 \quad &+ B_2 rm2 \quad + B_3 r \quad + B_4 r\beta + 1 \quad + B_5 r - \beta + 1 \quad + B_6 r^3\\ &+ \frac{W_6 A_1}{W_1} r - \beta \quad a \le r \le b.\end{aligned} \tag{22}$$

Since u(r) is known, by integrating from the Eq. (18) one have:

$$\varphi(r) = C_4\left[B_1 r^{\beta_1} + B_2 r^{\beta_2} + B_3 r + B_4 r^{\beta+1} + B_5 r^{-\beta+1} + B_6 r^3 + \frac{W_6 A_1}{W_1} r^{-\beta}\right]$$
$$+C_7\left[\frac{B_1}{\beta_1} r^{\beta_1} + \frac{B_2}{\beta_2} r^{\beta_2} + B_3 r + \frac{B_4}{\beta+1} r^{\beta+1} + \frac{B_5}{-\beta+1} r^{-\beta+1} + \frac{B_6}{3} r^3 + \frac{W_6 A_1}{W_1(-\beta)} r^{-\beta}\right] \quad (23)$$
$$+\frac{p_{11}^0}{g_{11}^0}\left(\frac{w_1^i}{-\beta+1} r^{-\beta+1} + w_2^i r\right) - \frac{A_1}{g_{11}^0 \beta} r^{-\beta} + A_2,$$

where A_2 is an unknown constant. Substituting Eq. (22) into Eqs. (19), the stresses of the inner FGPM layer are obtained as:

$$\boldsymbol{\sigma_r = C_1 r^{\beta}\left[B_1\beta_1 r^{\beta_1-1} + B_2\beta_2 r^{\beta_2-1} + B_3 + B_4(\beta+1) r^{\beta} + B_5(1-\beta) r^{-\beta} + 3B_6 r^2 - \beta W_6 A_1 r^{-\beta-1}/W_1\right]}$$
$$\boldsymbol{+C_2 r^{\beta}\left[B_1 r^{\beta_1-1} + B_2 r^{\beta_2-1} + B_3 + B_4 r^{\beta} + B_5 r^{-\beta} + B_6 r^2 + W_6 A_1 r^{-\beta-1}/W_1\right] - C_4 A_1/r} \quad (24)$$
$$\boldsymbol{+(C_3 r^{\beta} - \lambda_1^0 r^{2\beta})(w_1^i r^{-\beta} + w_2^i),,}$$
$$\boldsymbol{+C_5 r^{\beta}\left[B_1 r^{\beta_1-1} + B_2 r^{\beta_2-1} + B_3 + B_4 r^{\beta} + B_5 r^{-\beta} + B_6 r^2 + W_6 A_1 r^{-\beta-1}/W_1\right] - C_7 A_1/r}$$
$$\boldsymbol{+(C_6 r^{\beta} - \lambda_2^0 r^{2\beta})(w_1^i r^{-\beta} + w_2^i),.}$$

The mechanical and electrical boundary conditions can be expressed as (superscript ip, op and fgm denotes parameters in the inner FGPM, outer FGPM and FGM layers respectively):

$$\sigma_r^{ip}\big|_{r=a} = -p_i, \varphi^{ip}\big|_{r=a} = \varphi_a, \varphi^{ip}\big|_{r=b} = \varphi_b,$$
$$\sigma_r^{op}\big|_{r=d} = -p_o, \varphi^{op}|_{r=c} = \varphi_c, \varphi^{op}|_{r=d} = \varphi_d, \quad (25)$$

The continuity conditions for perfectly bonded layers can be expressed as:

$$\sigma_r^{ip}\big|_{r=b} = \sigma_r^{fgm}\big|_{r=b} \sigma_r^{op}\big|_{r=c} = \sigma_r^{fgm}\big|_{r=c}$$
$$u_r^{ip}\big|_{r=b} = u_r^{fgm}\big|_{r=b} u_r^{op}\big|_{r=c} = u_r^{fgm}\big|_{r=c} \quad (26)$$

Ten unknown coefficients (four A_1, A_2, B_1 and B_2 coefficients for inner FGPM layer and also four coefficients for outer FGPM layer and D_1 and D_2 for FGM layer) can be found by mechanical and electrical boundary conditions and continuity conditions. Concerning each of the boundary condition types, the system of linear algebraic equations for the resulted constants can be solved.

3. NUMERICAL RESULTS AND DISCUSSIONS

Considering numerical calculations, material constants for the hybrid hollow cylinder are listed in Table 1 [15, 16]. The hybrid hollow cylinder with internal radius a =0.6 m and external radius d=1 m is considered that rotates at the constant angular velocity ω=6π. The thickness of each FGPM layer is 0.02 m. The thermal boundary condition is considered as T0=50 K. The other corresponding boundary conditions are expressed as:

$$P_i = 1 \times 10^9 Pa, P_o = 0, \phi_a = 0, \phi_b = 0, \phi_c = 0, \phi_d = 0. \tag{27}$$

The following non-dimensional quantities are introduced:

$$R = \frac{r-a}{d-a}, u^* = \frac{u(r)}{a}, \sigma_j^* = \frac{\sigma_j}{P_i}, (j = r, \theta). \tag{28}$$

Table 1. Material constants

FGM				
E_0 (GPa)	α_0 (1/K)		k_{fgm} (W/mK)	$\boldsymbol{\rho_f^0(kg/m^3)}$
125	10×10^{-6}		2.9	**7860**
FGPM				
$c_{11}^0(GPa)$	$c_{12}^0(GPa)$	$c_{22}^0(GPa)$	$e_{11}^0(C/m^2)$	$\boldsymbol{e_{12}^0(C/m^2)}$
139	78	139	15.1	**-5.2**
k_i (W/mK)	k_0 (W/mK)	$P_{11}^0(C^2/m^2k)$	$g_{11}^0(C^2/Nm^2)$	$\boldsymbol{\rho_p^0(kg/m^3)}$
1.5	1.5	-3.2×10^{-5}	5.6×10^{-9}	**7750**
$\alpha_r^0(1/K)$	$\alpha_\theta^0(1/K)$	$h(W/m^2K)$		
8.53×10^{-6}	1.99×10^{-6}	0.82		

The effect of gradient index (β) of FGPM layers on the behavior of FGM cylinder is presented in Figs. 2-4. According to figures, interface continuity conditions and the boundary conditions are satisfied. The radial stress and displacement are decreasing with the decreasing of β. The influence of gradient index on the displacement is greater than on the stresses. So, the stresses and displacement in FGM layer can be controlled more effectively by using functionally graded piezoelectric material with proper gradient index. According to Fig. 3, the circumferential stress in FGM layer is decreasing with the decreasing of β and this is conversely in inner FGPM layer.

The effect of gradient index (η) of FGM layer on the behavior of hybrid cylinder is presented in Figs. 5,6. Fig. 5 depicts the distribution of radial stress along the radius for different values of η. As can be seen the radial stresses at the internal and the external surfaces of the hollow rotating cylinder satisfy the given boundary conditions. Moreover, the magnitude of the radial stress is increased as η is increased. It can be seen from Fig. 6 that the hoop stress along the radius decreases for η<1 and increases for η>1 as the radius increases. The hoop stress in FGM cylinder decreases with increasing η for the inner surface and conversely increases for the outer surface. Also, the hoop stress in FGPM layers increase with increasing η.

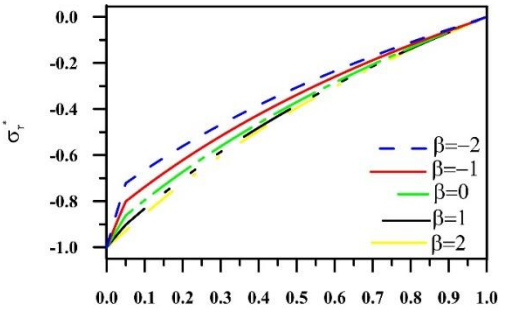

Fig. 2 Variations of radial stress distributions for different β, η=1.5

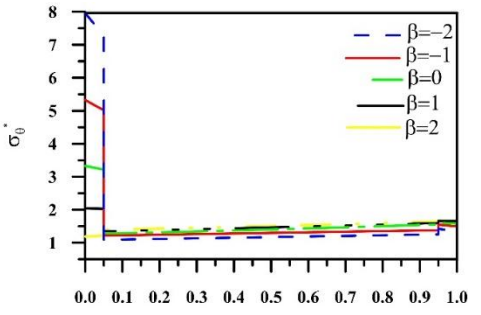

Fig. 3 Variations of circumferential stress distributions for different β, η=1.5

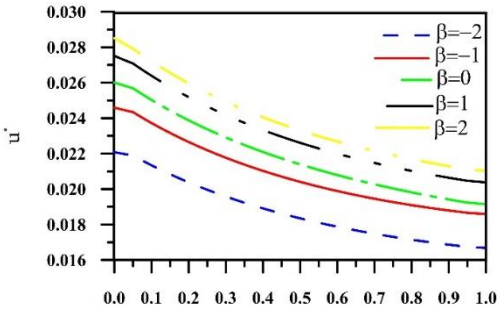

Fig. 4 Variations of displacement distributions for different β, η=1.5

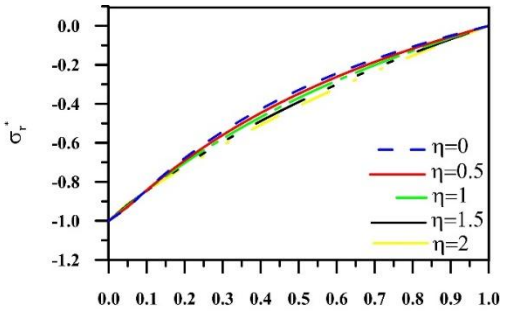

Fig. 5 Variations of radial stress distributions for different η, β =1.5

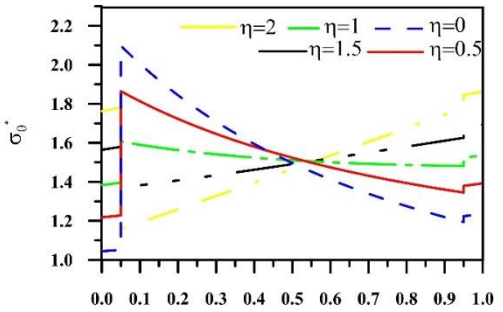

Fig. 6 Variations of circumferential stress distributions for different η, β =1.5

Figs. 7,8 show the stresses in the hybrid cylinder with different angular velocity. It can be observed the circumferential stress was increasing with the increasing of ω. Also it can be observed that the influence of angular velocity on the radial stress is negligible.

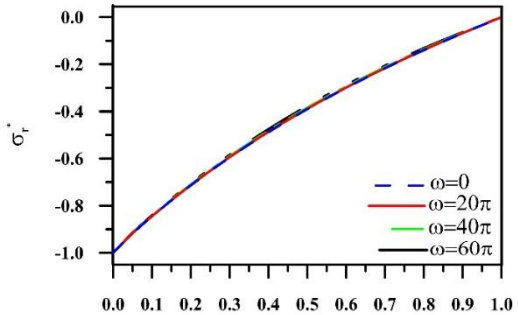

Fig. 7 Variations of radial stress distributions for different ω, η=1.5, β =1.5

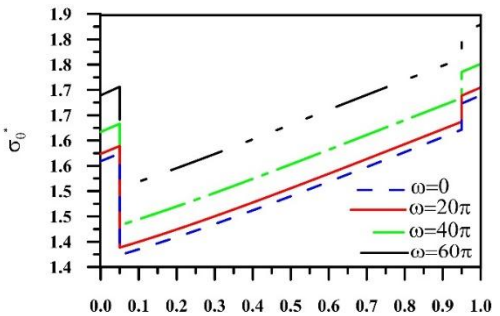

Fig. 8 Variations of circumferential stress distributions for different ω, η=1.5, β =1.5

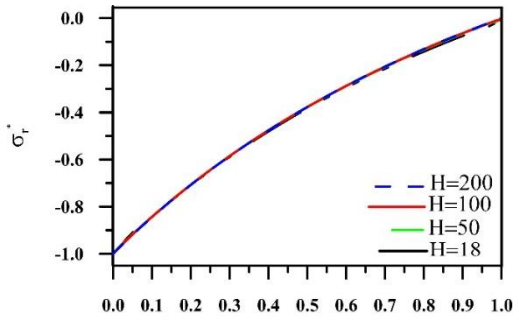

Fig. 9. Effect of thickness ratio on the radial stress distributions, η=1.5, β =1.5

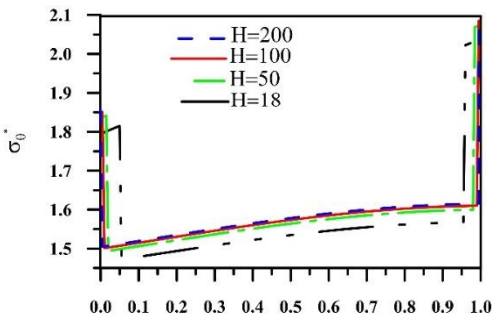

Fig. 10. Effect of thickness ratio on the circumferential stress distributions, η=1.5, β =1.5

The influence of FGPM layers thickness on the mechanical behavior of FGM cylinder is shown in Figs. 9,10. In this case, the internal pressure is considered as $P_i = 1 \times 10^8 Pa$. All other conditions are the same as before. For different thickness ratio (H), defined as the ratio of FGM layer thickness to FGPM layers thickness, the stresses are drawn. As the figures show, with decreasing the thickness of FGPM layers, the influence of FGPM layers without electric excitation decreases.

The effect of applied voltage (in unit of Volt) on the stresses and displacement of the cylinder under mechanical load is depicted in Fig. 11-13. In this case, the angular velocity ω=2π, $P_i = 1 \times 10^5 Pa$ and T_0=0 K. All other conditions are the same as before. According to the figures, the displacement and circumferential stress decrease by applying voltage in the inner FGPM layer and conversely increase by applying voltage in the outer FGPM layer. It can be seen that the displacement and circumferential stress are decreasing with increasing of applied voltage in the inner FGPM layer. So may one conclude that inner FGPM layer is more suitable than outer FGPM layer for using as the actuator. The induced strain of the FGPM actuator layer caused by applied voltage can change the stress and displacement distributions of the cylinder. According to the figures, the values of mechanical quantities can be control by applying voltage in actuator layer. Also, it is seen that the influence of variation of applied voltage on the displacement is greater than the one on the stresses.

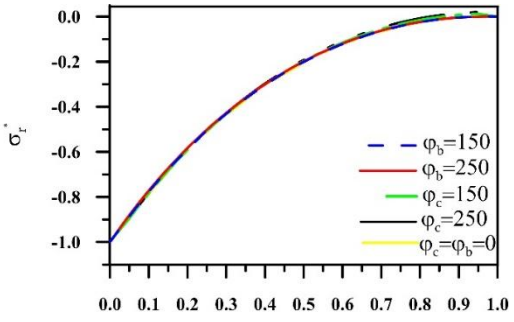

Fig. 11 Influence of applied voltage on the radial stress distributions, η=1, β =1.5

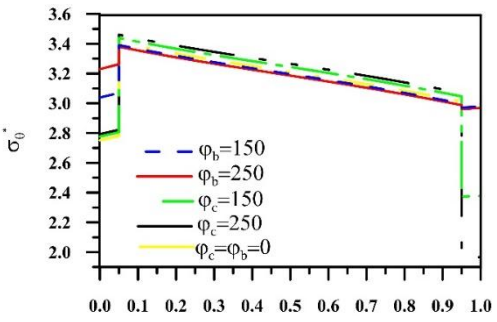

Fig. 12 Influence of applied voltage on the circumferential stress distributions, η=1, β =1.5

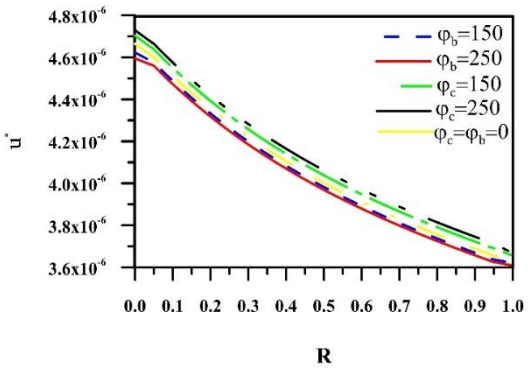

Fig. 13 Influence of applied voltage on the displacement distributions, η=1, β =1.5

4. CONCLUSIONS

This paper presents an analytical solution for the thermo-electro-elastic behavior of a rotating, infinitely long hollow FGM cylinder with FGPM layers bonded to its inner and outer surfaces. All mechanical and thermal properties, except for Poisson's ratio, are assumed to vary as power functions of the radius. The analytical results provide valuable insights into the effects of various parameters on the response of the hybrid cylinder. Based on the numerical evaluation of the solution, the following conclusions are drawn:

- **Effect of Gradient Index β\beta:** Both stresses and displacement in the FGM layer decrease as β\beta decreases. This indicates that stresses and displacement can be more effectively controlled by selecting an appropriate gradient index for the FGPM material. The gradient index has a more pronounced effect on displacement than on stresses.
- **Effect of Gradient Index η\eta:** In the FGM cylinder, the hoop stress decreases with increasing η\eta at the inner surface but increases at the outer surface.
- **Effect of Angular Velocity ω\omega:** Circumferential stress increases with an increase in angular velocity.
- **Effect of FGPM Layer Thickness:** As the thickness of the FGPM layers decreases, the influence of these layers on the behavior of the cylinder without electric excitation diminishes.
- **Actuator Suitability:** The inner FGPM layer is more effective as an actuator compared to the outer layer. Displacement and circumferential stress decrease with increasing applied voltage in the inner FGPM layer. By applying voltage to the actuator layer, mechanical quantities such as displacement and stress can be controlled. Furthermore, the effect of applied voltage on displacement is greater than its effect on stresses.

Transparency Statement

The data supporting this study are available upon reasonable request to the corresponding author, subject to ethical and confidentiality considerations.

Acknowledgments

We would like to express our gratitude to all individuals who contributed to this project.

Declaration of Interest

The authors declare that they have no competing interests.

Funding

This research received no specific grant from any funding agency, commercial, or not-for-profit sectors.

REFRENCESS

[1] Alibeigloo, A. (2009). Static analysis of a functionally graded cylindrical shell with piezoelectric layers as sensor and actuator. Smart Materials and Structures, 18(6), 065004. https://doi.org/10.1088/0964-1726/18/6/065004

[2] Alibeigloo, A., & Nouri, V. (2010). Static analysis of functionally graded cylindrical shell with piezoelectric layers using differential quadrature method. Composite Structures, 92(7), 1775–1785. https://doi.org/10.1016/j.compstruct.2010.02.004

[3] Liew, K. M., He, X. Q., Ng, T. V., & Kitipornchai, S. (2002). Active control of FGM shells subjected to a temperature gradient via piezoelectric sensor/actuator patches. International Journal for Numerical Methods in Engineering, 55(6), 653–668. https://doi.org/10.1002/nme.519

[4] He, X. Q., Liew, K. M., Ng, T. Y., & Sivashankar, S. (2002). A FEM model for the active control of curved FGM shells using piezoelectric sensor/actuator layers. International Journal for Numerical Methods in Engineering, 54(6), 853–870. https://doi.org/10.1002/nme.451

[5] Wang, H. M. (2011). Dynamic electromechanical behavior of a triple-layer piezoelectric composite cylinder with imperfect interfaces. Applied Mathematical Modelling, 35(4), 1765–1781. https://doi.org/10.1016/j.apm.2010.10.008

[6] Shen, H. S., & Noda, N. (2007). Postbuckling of pressure-loaded FGM hybrid cylindrical shells in thermal environments. Composite Structures, 77(4), 546–560. https://doi.org/10.1016/j.compstruct.2005.08.006

[7] Aghaei Khafri, M., & Saadatfar, M. (2013). Analytical solution for thermo-electro-elastic stress in FGM hollow cylinder with functionally graded piezoelectric layers. Proceedings of ISME. Iran.

[8] El-Naggar, A. M., Abd-Alla, A. M., Fahmy, M. A., & Ahmed, S. M. (2002). Thermal stresses in a rotating non-homogeneous orthotropic hollow cylinder. Heat and Mass Transfer, 39(1), 41–46. https://doi.org/10.1007/s00231-001-0285-4

[9] Eraslan, A. N., & Akis, T. (2006). On the plane strain and plane stress solutions of functionally graded rotating solid shaft and solid disk problems. Acta Mechanica, 181(1–2), 43–63. https://doi.org/10.1007/s00707-005-0276-5

[10] Saadatfar, M., Iravani, Y., & Sajjadi, S. M. (2022). The effect of inhomogeneity coefficient for stress distribution in a FGM two-layer disc with variable velocity. The 30th Annual International Conference of the Iranian Association of Mechanical Engineers. (In Persian).

[11] Saadatfar, M., Iravani, Y., & Sajjadi, S. M. (2022). Stress analysis of a porous functionally graded magneto-electro-elastic rotating cylinder rested in an elastic foundation. The Annual Conference on Smart Materials and Structures. (In Persian).

[12] Dai, H. L., Hong, L., Fu, Y. M., & Xiao, X. (2010). Analytical solution for electro-magneto-thermo-elastic behaviors of a functionally graded piezoelectric hollow cylinder. Applied Mathematical Modelling, 34(2), 343–357. https://doi.org/10.1016/j.apm.2009.04.008

[13] Jabbari, M., Sohrabpour, S., & Eslami, M. R. (2002). Mechanical and thermal stresses in a functionally graded hollow cylinder due to radially symmetric loads. International Journal of Pressure Vessels and

Piping, 79(7), 493–497. https://doi.org/10.1016/S0308-0161(02)00043-1

[14] Saadatfar, M., & Razavi, A. S. (2009). Piezoelectric hollow cylinder with thermal gradient. Journal of Mechanical Science and Technology, 23(1), 47–55. https://doi.org/10.1007/s12206-008-1002-8

[15] Alibeigloo, A. (2008). Static analysis of an anisotropic laminated cylindrical shell with piezoelectric layers using differential quadrature method. Journal of Mechanical Engineering Science, 222(5), 865–880. https://doi.org/10.1243/09544062JMES866

[16] Xiang, H. J., & Shi, Z. F. (2009). Static analysis for functionally graded piezoelectric actuators or sensors under a combined electro-thermal load. European Journal of Mechanics - A/Solids, 28(2), 338–346. https://doi.org/10.1016/j.euromechsol.2008.06.007